Model Reference Adaptive Controller for Grid-Forming Inverters applied to Single-Phase Microgrid

Vítor Paese De Carli *
* Grupo de Eletrônica de Potência e Controle, Universidade Federal de Santa Maria - Santa Maria, Brazil

***Abstract*—This paper features the use of a model reference adaptive controller (MRAC) for the inner loop of a grid-forming inverter (GFM). The gradient algorithm is based on the discrete-time model of the converter and its state variables feedback. An adaptive control law is particularly suitable for a GFM due to its high parameter uncertainties. During island operation, the load impedance could vary from open circuit to its nominal load, and when connected to the main grid, the impedance at the point of common coupling (PCC) is also unknown.**

***Index Terms*—MRAC, grid-forming, microgrid, droop.**

I. Introduction

Distributed energy resources (DERs) are playing an increasingly significant role in the electrical power system, gradually replacing synchronous generators [1]. This change reduces the system's inertia and increases intermittent power resources. In a system dominated by generators, frequency stability is determined by the kinetic energy stored in the generator's mechanical components [2]. However, in a grid highly reliant on inverters, frequency regulation is poor. So, reducing system inertia may lead to oscillations that decrease its reliability.

Typically, there are two primary types of inverter control used for distributed generation: grid-following (GFL) and grid-forming (GFM) [3]. Currently, the predominant type of inverter is the GFL inverter, which functions as a current source and relies on the electrical grid to determine its frequency and angle references. On the other hand, GFM-controlled inverters operate as voltage sources and have amplitude and angle references based on active and reactive power references.

To operate in a 100% inverter-based grid, at least one GFM inverter is necessary since the voltage and frequency reference must be defined. Besides this significant advantage, grid-forming inverters also enable the integration of Renewable Energy (RE) into a microgrid (MG) and increase grid resilience by assisting in frequency regulation.

In [4], the strategy of using MGs to relieve congestion points in the North American transmission and distribution electrical system is discussed. Additionally, the use of MGs for emergency operation due to natural phenomena that may compromise the main grid is addressed. In other words, when the main grid is inoperative, the MG, through a black start, can quickly restore the grid and, combining the generation of other RES in GFL mode, can take on critical loads.

In this context, this article proposes implementing an adaptive control strategy to deal with the uncertainties present in a single-phase MG. The MRAC controller is well-suited for this purpose, as a GFM inverter can function in islanded mode with no load or its nominal load, as well as in connected mode exporting power. The plant model considers an LC Filter and an RL load and is developed in discrete time while accounting for transportation delay. Additionally, the proposed controllers are elaborated, and the system is simulated in Virtual Hardware-in-the-Loop (VHIL) for validation purposes.

II. Modeling of the Microgrid

The proposed system consists of a single-phase microgrid with two grid-forming inverters that share a load of apparent power $S = 30$ kVA and operate at a power factor $FP = 0.8$. The MG can also switch between islanded and grid-connected modes using the STS switch. The system is exhibited in Figure 1.

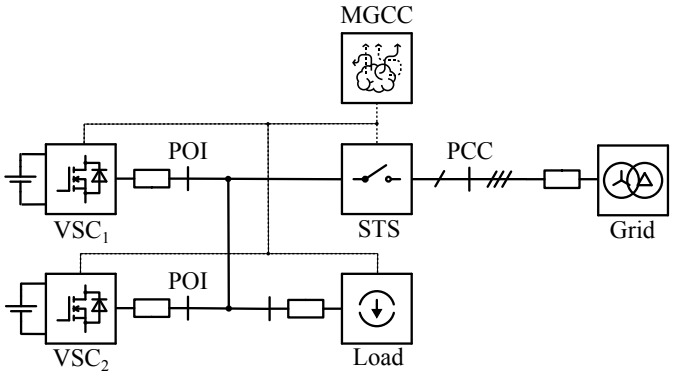

Figure 1. Proposed single-phase Microgrid.

Considering an LC filter and a load with an inductive power factor, the converters VSC_1 and VSC_2 may be modeled according to Figure 2 if the output of the other converters in the MG is disregarded and treated as an exogenous disturbance.

The state space model in the continuous time domain considering the capacitor voltage as its output is given by:

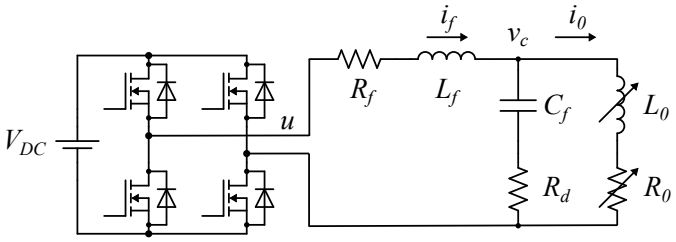

Figure 2. Grid-Forming Topology.

$$\begin{bmatrix} \dot{i_f} \\ \dot{v_c} \\ \dot{i_0} \end{bmatrix} = \begin{bmatrix} -\frac{R_f+R_d}{L_f} & -\frac{1}{L_f} & \frac{R_d}{L_f} \\ \frac{1}{C_f} & 0 & -\frac{1}{C_f} \\ \frac{R_d}{L_0} & \frac{1}{L_0} & -\frac{R_0+R_d}{L_0} \end{bmatrix} \begin{bmatrix} i_f \\ v_c \\ i_0 \end{bmatrix} + \begin{bmatrix} \frac{1}{L_f} \\ 0 \\ 0 \end{bmatrix} u$$
$$y = \begin{bmatrix} 0 & 1 & 0 \end{bmatrix} \cdot \begin{bmatrix} i_f \\ v_c \\ i_0 \end{bmatrix} \tag{1}$$

The model may also be presented in its compact form as in (2).

$$\begin{aligned} \dot{\mathbf{x}} &= \mathbf{A}\mathbf{x} + \mathbf{B}u \\ y &= \mathbf{C}x \end{aligned} \tag{2}$$

As the control law will be implemented in a digital system, the model should be discretized for better reliability. The discrete-time model using a Zero-Order Hold (ZOH) may be written in compact form as follows

$$\begin{aligned} \mathbf{x}[k] &= \mathbf{A_d}\mathbf{x}[k-1] + \mathbf{B_d}u[k-1] \\ y[k] &= \mathbf{C}\mathbf{x}[k] \end{aligned} \tag{3}$$

where the matrices $\mathbf{A_d}$ and $\mathbf{B_d}$ are given by equations (4) and (5), respectively.

$$\mathbf{A_d} = e^{\mathbf{A}T_s} \tag{4}$$

$$\mathbf{B_d} = (\mathbf{A_d} - \mathbf{I})\mathbf{A}^{-1}\mathbf{B} \tag{5}$$

The model should also account for transport delay. To achieve this, an augmented state space system is created by introducing the new state ϕ, which represents a one-sample delay. The final equation is presented in (6).

$$\begin{bmatrix} i_f[k] \\ v_c[k] \\ i_0[k] \\ \phi[k] \end{bmatrix} = \begin{bmatrix} \mathbf{A_d} & \mathbf{B_d} \\ \mathbf{0} & \mathbf{0} \end{bmatrix} \begin{bmatrix} i_f[k-1] \\ v_c[k-1] \\ i_0[k-1] \\ \phi[k-1] \end{bmatrix} + \begin{bmatrix} 0 \\ 0 \\ 0 \\ 1 \end{bmatrix} u[k-1]$$
$$y[k] = \begin{bmatrix} 0 & 1 & 0 & 0 \end{bmatrix} \begin{bmatrix} i_f[k] \\ v_c[k] \\ i_0[k] \\ \phi[k] \end{bmatrix} \tag{6}$$

$$\begin{aligned} \mathbf{x}[k] &= \mathbf{A_{d_\phi}}\mathbf{x}[k-1] + \mathbf{B_{d_\phi}}u[k-1] \\ y[k] &= \mathbf{C_{d_\phi}}\mathbf{x}[k] \end{aligned} \tag{7}$$

By applying the transformation from state space to transfer function given by (8), the equation that relates the output capacitor voltage v_c with the control action u is presented in (9).

$$G(z) = \mathbf{C_{d_\phi}}(z\mathbf{I} - \mathbf{A_{d_\phi}})^{-1}\mathbf{B_{d_\phi}} \tag{8}$$

$$G(z) = \frac{V_c(z)}{U(z)} = \frac{\beta_2 z^2 + \beta_1 z + \beta_0}{z^4 + \alpha_3 z^3 + \alpha_2 z^2 + \alpha_1 z + \alpha_0} \tag{9}$$

The discrete domain transfer function has a relative degree of $n_p = 2$, however, the undamped zero that occurs due to the discretization process appears at a high frequency close to z = -1. Therefore, this zero should be neglected for better performance of the proposed controller. If not, the MRAC may try to cancel it by the addition of a high-frequency pole, and for that to happen, a high oscillatory control action may be needed [5]. Due to these considerations, the model of the plant may be represented by

$$G(z) = G_0(z) + \mu\Delta_a(z) \tag{10}$$

where $G_0(z)$ represents the plant neglecting the sampling zero and $\mu\Delta_a(z)$ represents the neglected part.

Let the roots of the numerator of the transfer function $G(z)$ be the nominal zero z_0 and the sampling zero z_μ. Then $G_0(z)$ and $\mu\Delta_a(z)$ can be rewritten as follows:

$$\begin{aligned} G_0(z) &= \frac{K_1(z+z_0) + K_2}{z^4 + \alpha_3 z^3 + \alpha_2 z^2 + \alpha_1 z + \alpha_0} \\ \mu\Delta_a(z) &= \frac{K_3(z+z_\mu)^2}{z^4 + \alpha_3 z^3 + \alpha_2 z^2 + \alpha_1 z + \alpha_0} \end{aligned} \tag{11}$$

where $K_{1,3}$ represents the constants that must be found by taking the numerator part of (10) and solving equation (12).

$$\beta_2 z^2 + \beta_1 z + \beta_0 = K_1(z+z_0) + K_2 + K_3(z+z_\mu)^2 \tag{12}$$

By solving the equation, $K_{1,3}$ can be expressed in terms of nominal plant coefficients:

$$\begin{aligned} K_1 &= \beta_0 - \beta_2 z_\mu^2 - z_0(\beta_1 - 2\beta_2 z_\mu) \\ K_2 &= \beta_1 - 2\beta_2 z_\mu \\ K_3 &= \beta_2 \end{aligned} \tag{13}$$

Finally, Figure 3 displays the bode diagram for the nominal plant $G(z)$, the simplified plant G_0, and the non-modeled dynamics $\mu\Delta_a(z)$. This analysis considers the specifications outlined in Table I.

III. Inner Loop Voltage Controller

This section introduces the full-state feedback gradient adaptive control law and the approach used to adjust the gain and phase of the reference model for a single-phase system.

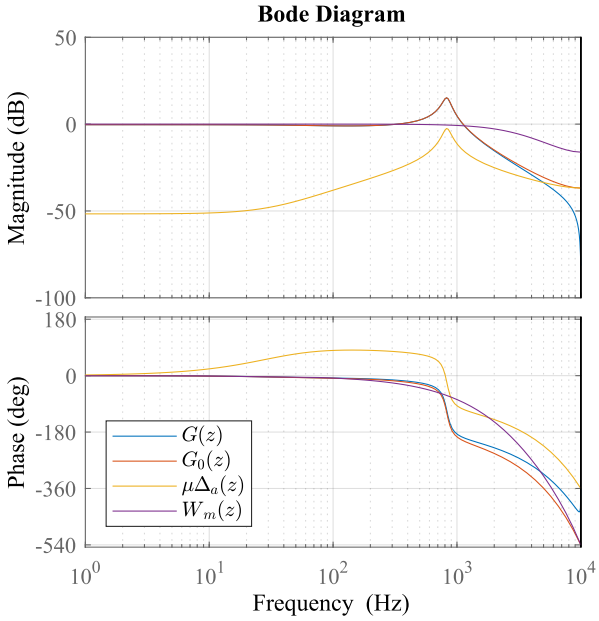

Figure 3. Bode Diagram of the Nominal Plant, Simplified Plant, Non-modeled Dynamics and Reference Model.

Table I
VSC_1 AND VSC_2 SPECIFICATIONS

Parameter	Symbol	Value
Filter Inductance	L_f	1 mH
Filter Parasitic Resistance	R_f	0.1 Ω
Filter Capacitance	C_f	44 μF
Damping Resistance	R_d	0.5 Ω
Load Resistance	R_0	2.58 Ω
Load Inductance	L_0	5.1 mH
Grid Nominal Voltage	V_{RMS}	220 V
Grid Nominal Frequency	ω_0	2π60 rad/s
DC Bus Voltage	V_{DC}	500 V

A. MRAC

The MRAC controller is designed to track the output of the reference model $W_m(z)$ by adjusting the parameter vector denoted as $\boldsymbol{\theta}$ as illustrated in Figure 4. The control law is based on a gradient algorithm and involves feedback from all states shown in equation (6).

An MRAC controller requires a reference model $W_m(z)$ with the same relative order n_p as the controlled plant. Taking into consideration the previous points, $W_m(z)$ should be chosen to have a third-order relative to match the simplified plant $G_0(z)$. $W_m(z)$ is shown in equation (14), in which the poles $p_{1,3}$ should be selected according to the required dynamics, and the numerator is selected to match unitary gain. Its bode plot can be found in Figure 3.

$$W_m(z) = \frac{(1-p_1)(1-p_2)(1-p_3)}{(z-p_1)(z-p_2)(z-p_3)} \tag{14}$$

Considering Backward Euler approximation, the discrete-time control action that produces the required effect, i.e. tracks

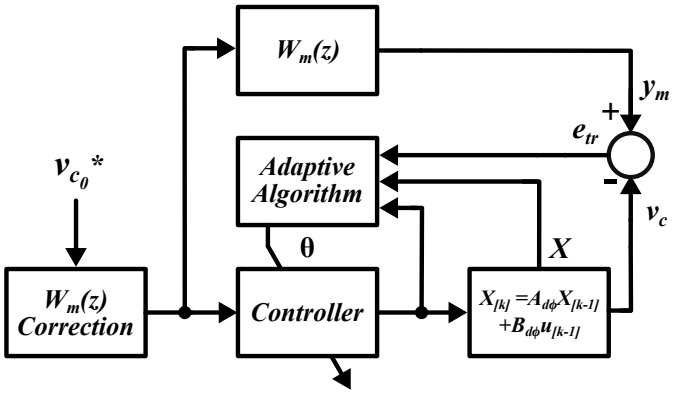

Figure 4. MRAC Block Diagram.

the reference model, is given by:

$$u[k] = \boldsymbol{\theta}^T[k]\boldsymbol{\omega}[k] \tag{15}$$

where $\boldsymbol{\theta}$ and $\boldsymbol{\omega}$ are defined as:

$$\boldsymbol{\theta}[k] = \boldsymbol{\theta}[k-1] - \frac{T_s\gamma\varepsilon[k-1]\boldsymbol{\zeta}[k-1]}{m^2[k-1]} \tag{16}$$

$$\boldsymbol{\omega}[k] = \begin{bmatrix} i_f & v_c & i_0 & \phi & v_c^* & d_{sin} & d_{cos} \end{bmatrix}^T[k] \tag{17}$$

The vector $\boldsymbol{\zeta}$ has the same dimension as $\boldsymbol{\omega}$ ($\boldsymbol{\zeta} \in \mathbb{R}^{7\times1}$) and its computation is performed by filtering $\boldsymbol{\omega}$ with the reference model $W_m(z)$:

$$\boldsymbol{\zeta}[k] = W_m(z)\boldsymbol{\omega}[k] \tag{18}$$

Furthermore, the augmented error ε is calculated by summing the tracking error e_{tr}, the product of $\boldsymbol{\theta}$ and $\boldsymbol{\zeta}$, and the control action u filtering.

$$\varepsilon[k] = e_{tr}[k] + \xi[k] \tag{19}$$

$$e_{tr}[k] = v_c[k] - y_m[k] \tag{20}$$

$$\xi[k] = \boldsymbol{\theta}^T[k]\boldsymbol{\zeta}[k] - W_m(z)u[k] \tag{21}$$

The normalizing factor m^2 mentioned in (16) must be detailed. Its purpose is to slow down the convergence of the gradient algorithm, especially when the derivatives of the involved variables are too large. This improves the stability of the control law and it is done by the computation of m^2 as follows:

$$m^2[k] = 1 + \boldsymbol{\zeta}^T[k]\boldsymbol{\zeta}[k] + \xi[k]^2 \tag{22}$$

As the converter can be connected in parallel with other sources, its control law must also include the rejection of disturbances. This is achieved by incorporating d_{sin} and d_{cos} into $\boldsymbol{\omega}$: d_{sin} represents the 60 Hz voltage component measured at the point of interconnection (POI), while d_{cos} represents the same variable shifted by 90º.

Lastly, a step-by-step procedure for implementing the proposed MRAC in a discrete physical system is presented:

1) Measure all the states of the plant.
2) Correct magnitude and phase of $W_m(z)$ as presented in the next section and compute $y_m[k]$.
3) Compute $\boldsymbol{\zeta}[k]$.
4) Compute $\boldsymbol{\theta}[k]$.
5) Compute $u[k]$.
6) Compute $\varepsilon[k]$.
7) Compute $m^2[k]$.
8) Update the control action u at the digital-to-analog converter and wait for the next Interrupt-Service-Routine.

B. Model Reference Correction

As mentioned previously, the main goal of an MRAC Controller is to track the output of a reference model. The choice of a unitary reference model is not achievable by any physical hardware, so a slower reference model must be chosen. A feasible reference model has non-negligible gain and phase deviation which need to be corrected.

A very widespread approach in the literature [6] is the use of the transformation given by:

$$v_c^* = \frac{1}{\rho_m}(cos(\theta_m)v_{c_\alpha}^* + sin(\theta_m)v_{c_\beta}^*) \tag{23}$$

where ρ_m and θ_m represent the magnitude and phase shift of the discrete reference model, respectively. Moreover, the variables $v_{c_\alpha}^*$ and $v_{c_\beta}^*$ are the reference given by the primary controller and have been filtered, so that β component is shifted by 90º.

In a three-phase system, the α and β components can be obtained using Clarke transformation. However, this method does not apply to a single-phase system. To work around this issue, the primary controller signal can be passed through a second-order generalized integrator (SOGI). To maintain adaptability, a Frequency-Locked-Loop (FLL) is also implemented to allow the filter to change its resonance frequency, thereby compensating for any frequency deviation led by the droop controller. The equivalent block diagram of the structure is shown in Figure 5.

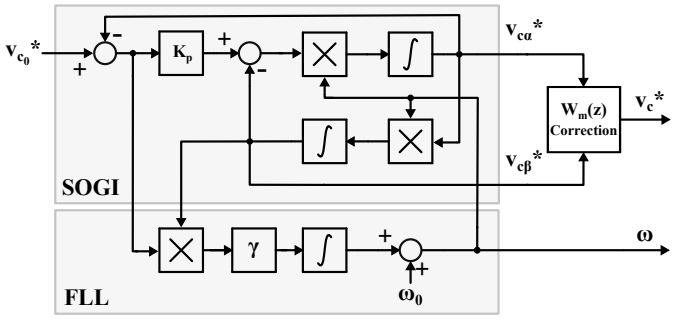

Figure 5. Reference Model Correction.

IV. Primary Control

In a grid-forming inverter, the primary control's main goal is to generate the voltage reference for the inner loops. In simpler terms, the primary control needs to provide the magnitude and angle for the voltage control loop so that the inverter acts like a phasor voltage source.

For the system, the selected controller to obtain such a result is the droop controller with two integrators. The droop is meant to mimic the operation of a synchronous generator in which the imbalance between the input kinetic energy and the exported electrical energy produces variations in the magnitude and frequency of the output voltage.

The droop mechanism is based on the principle of large generators with predominant inductive output impedance. However, this principle does not hold true for inverter-based resources, particularly in low-voltage systems where the grid impedance is mostly resistive. Thus, power-sharing is poor, and an improved droop must be implemented to make the system more independent of the grid parameters [7]. Figure 6 displays the block diagram of the droop controller with two integrators.

Another widely spread resource to improve the performance is the usage of a virtual impedance [8]. This method involves measuring the output current of the converter i_0 and subjecting it to a virtual inductive impedance. The voltage drop across this impedance is subtracted from the output signal of the improved droop, which helps to approximate the output impedance of the converter to the output impedance of a synchronous generator [9].

In the frequency domain, a virtual impedance is represented by:

$$Z_{V_0} = R_v + sL_v \tag{24}$$

A transfer function with only one zero, considered improper, results in a non-causal system when implemented in discrete time. The implementable function can be observed in(25).

$$Z_V(s) = \frac{(R_v + sL_v)\cdot\omega_p^2}{s^2 + 2\zeta_p\omega_p s + \omega_p^2} \tag{25}$$

The addition of high-frequency poles can cause degradation in the response due to the inherent noise of the physical measurement system. Therefore, a low-pass filter (LPF) is added in series with Z_V to ensure that the loop does not operate at high frequencies. Figure 7 shows the bode diagram of the ideal virtual impedance, the achievable virtual impedance Z_V, and Z_V in series with the LPF. It is evident that near the frequency of interest ω_0, there is no significant difference in magnitude and the phase degradation is minimal.

V. Simulation Results

To validate the system, the simulation was conducted in VHIL using the Typhoon HIL Control Center software. The control law was developed in C code, and the transfer functions projected in continuous time were discretized using the Tustin Method. A simulation step of 0.25 µs was selected. The

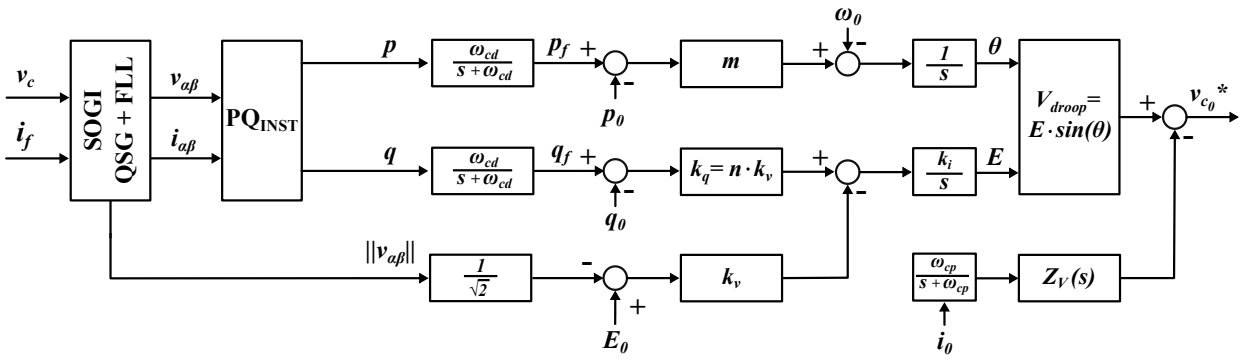

Figure 6. Primary Control Block Diagram.

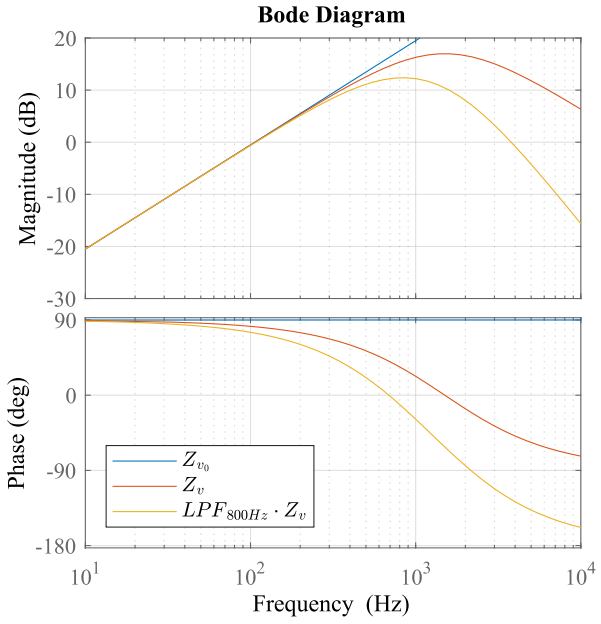

Figure 7. Bode Diagram of $Z_V(s)$, $Z_{V_0}(s)$ and $LPF_{800Hz} \cdot Z_{V_0}(s)$.

results for connected and islanded mode based on load variation will be presented in the following sections considering the control parameters outlined in Table II.

A. Islanded Mode

The system was tested in islanded mode, i.e. VSC_1 and VSC_2 are in parallel and STS switch is open. In this scenario, both inverters, sized for the same capacity of $S_{nom} = 15kVA$, share a time-variant load that is equally distributed between them. Figure 8 illustrates the performance of VSC_1 as the load parameters R_0 and L_0 vary from open-circuit to nominal load, considering both inductive and capacitive power factor. It is important to notice that the tracking error remains satisfactory throughout all operations, even with a load ramp.

B. Grid-Connected Mode

The performance of the controllers was further validated under grid-connected operation. In this context, VSC_1, VSC_2,

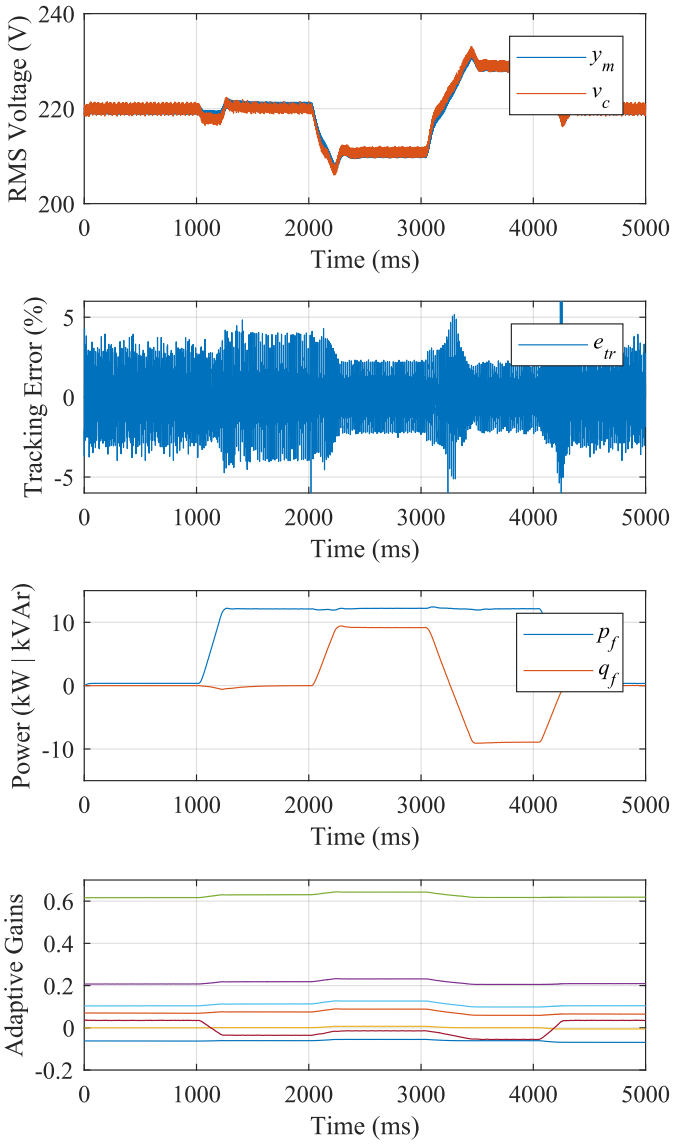

Figure 8. Simulation Results for Islanded Mode.

Table II
CONTROL PARAMETERS

Parameter	Symbol	Value
MRAC		
Sampling Frequency	f_s	20 kHz
Reference Model Poles	$p_{1,3}$	0.3
Adaptation Gain	γ	100
Magnitude Correction Gain	ρ_m	0.9995
Phase Correction Angle	θ_m	-5.35º
Droop		
Frequency-Watt Loop Gain	m	0.1 Hz/kW
Volt-VAr Loop Gain	n	1 V/kVAr
Integral Gain	k_i	5
Proportional Gain	k_v	5
Power LPF cutoff frequency	ω_{cd}	$2\pi 6$ rad/s
Virtual Impedance		
Virtual Resistance	R_v	0.1 mΩ
Virtual Inductance	L_v	2 mH
High-frequency Poles	ω_p	$2\pi 1500$ rad/s
Damping Coefficient	ζ_p	1
LPF cutoff frequency	ω_{cp}	800 Hz

and the grid operate in parallel, with the power exported by the converters being arbitrarily determined by the Microgrid Central Controller (MGCC). As the exported power setpoints are adjusted, the converters must dynamically modify their voltage and frequency references according to droop control principles. Additionally, the adaptation gains need to change to ensure that the required reference values are achieved effectively. Figure 9 presents the results for this scenario, demonstrating the system's response as the reference active and reactive power setpoints change. Notably, the tracking error remains below 2% throughout the entire test.

VI. CONCLUSION

This paper presents a model reference adaptive controller applied to the inner voltage loop of a single-phase grid-forming inverter. The increased use of distributed energy resources, particularly in low-voltage and household applications, demands the development of low-power systems that can manage both islanded and grid-connected operations. The main objective of this paper was to display the satisfactory performance of the MRAC as the grid parameters change.

Future research on similar systems should focus on developing strategies to address non-linear loads. A widespread approach for this issue is the implementation of multi-resonant controllers in parallel with the MRAC. Another significant challenge, especially in island mode, is the limitation of the output current during grid short circuits. To address this, a Fault Ride Through-like solution should be proposed in the absence of cascaded loops [10].

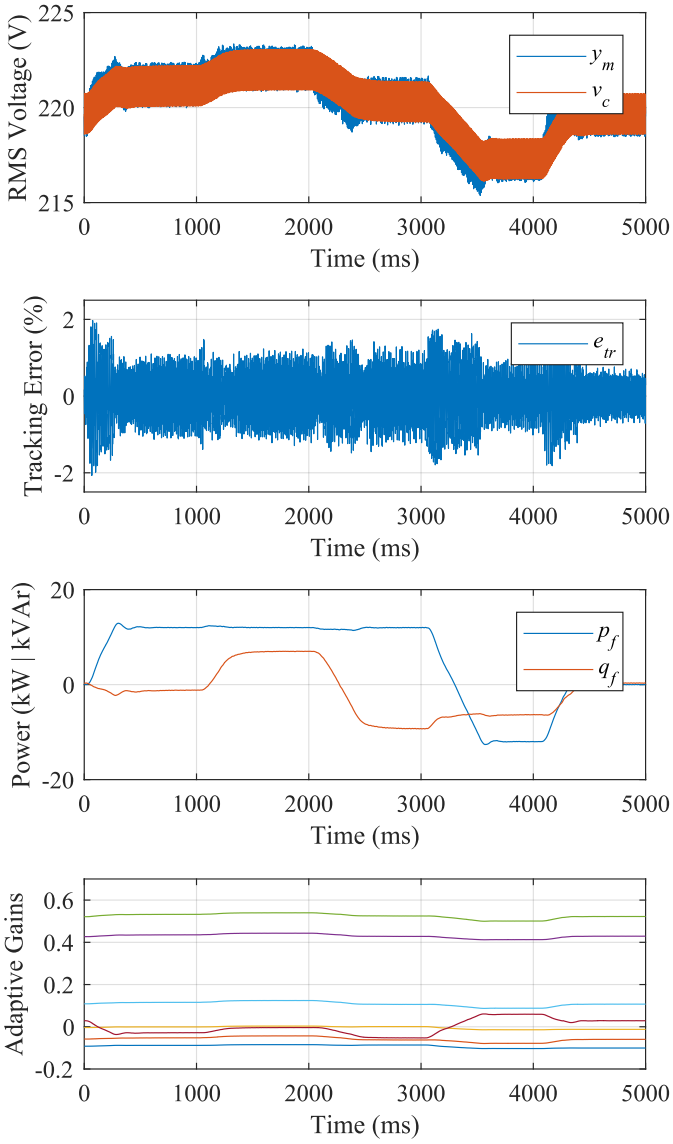

Figure 9. Simulation Results for Grid Connected Mode.

REFERENCES

[1] F. Milano *et al.*, "Foundations and challenges of low-inertia systems," *Power Systems Computation Conference*, 2018.

[2] Z. C. Robert H. Lasseter and D. Pattabiraman, "Grid-forming inverters: A critical asset for the power grid," *IEEE Journal of Emerging and Selected Topics in Power Electronics*, 2019.

[3] D. B. Rathnayake *et al.*, "Grid forming inverter modeling, control, and applications," *IEEE Access*, 2021.

[4] Y. P. Adam Hirsch and J. Guerrero, "Microgrids: A review of technologies, key drivers, and outstanding issues," *Renewable and Sustainable Energy Reviews*, 2018.

[5] H. A. G. Jorge Rodrigo Massing, Marcio Stefanello and H. Pinheiro, "Adaptive voltage control of grid-forming inverters," *IEEE Workshop on Computers in Power Electronics*, 2023.

[6] H. A. G. Jorge Rodrigo Massing, Márcio Stefanello and H. Pinheiro, "Adaptive current control for grid-connected converters with lcl filter," *2017 11th IEEE International Conference on Compatibility, Power Electronics and Power Engineering*, 2011.

[7] S. B. Zakaria Charfi and A. Tlemçani, "A comparison of control strategies for passivity-based vsi in microgrids between conventional droop control and droop control with two integrators," *2023 2nd International Conference on Electronics, Energy and Measurement*, 2023.

[8] X. Y. Sara Yahia Altahir and X. Liu, "A power sharing method for inverters in microgrid based on the virtual power and virtual impedance control," *2017 11th IEEE International Conference on Compatibility, Power Electronics and Power Engineering*, 2017.

[9] T.-L. L. Josep M. Guerrero, Mukul Chandorkar and P. C. Loh, "Advanced control architectures for intelligent microgrids—part i: Decentralized and hierarchical control," *IEEE Transactions on Industrial Electronics*, 2012.

[10] A. T. Pereira and H. Pinheiro, “Inner loop controllers for grid-forming converters,” *2022 14th Seminar on Power Electronics and Control*, 2022.